Flexural design of alkali-activated reinforced concrete beams: Evaluating model errors using standards for Portland concrete

Terms of use:

Publisher copyright

(Article begins on next page)

10 March 2025

ARTICLE

fib WILEY

Flexural design of alkali-activated reinforced concrete beams: Evaluating model errors using standards for Portland concrete

Erica Lenticchia[1] | Marialorenza Vescovi[2]

[1]Department of Structural, Geotechnical and Building Engineering, Politecnico di Torino, Torino, Italy

[2]Department of Engineering and Architecture, University of Parma, Parma, Italy

Correspondence
Erica Lenticchia, Department of Structural, Geotechnical and Building Engineering, Politecnico di Torino, C.so Duca degli Abruzzi 24, 10129 Torino, Italy.
Email: erica.lenticchia@polito.it

Abstract

The article examines the potential of utilizing existing standard codes, although originally designed for Portland cement, in the flexural design of geopolymer (GP) concrete beams. In particular, the article collects experimental data from the literature on the cracking and ultimate moment of reinforced GP concrete beams, with and without steel fibers (SFs). The experimental moments are compared with those calculated using different standard codes for Portland cement (2nd generation EC2, ACI318, ACI363, AS3600) and GP concrete (SATS199). The purpose of this comparison is to evaluate the model error obtained with the different codes. The same procedure is applied on experimental data from RC beams made with Portland cement. To study the model error, the results obtained with different precursor materials (granulated blast furnace slag or fly ash), concrete compressive strengths, and reinforcement percentages are analyzed. The different codes have different levels of conservatism, resulting in different average model errors. However, within the same code, the average model errors for GP and Portland concretes are similar. Therefore, the existing codes can be used to calculate the cracking moment and ultimate moment of GP concrete beams. However, some uncertainty remains for the ultimate moment of over-reinforced beams, for which the number of experimental data is still limited.

KEYWORDS

ACI318, ACI363, alkali-activated concrete, AS3600, beam, bending, cracking, design, Eurocode 2, geopolymer, SATS199

1 | INTRODUCTION

This study investigates the feasibility of using existing standard codes for ordinary concrete (OC) in Portland cement for the flexural design of geopolymer concrete (GPC) beams.

Portland cement is the most widely used material in civil engineering and is responsible for a significant amount of carbon dioxide emissions worldwide. To be precise, at least 8% of the world's annual human-made CO_2 emissions are attributed to its production.[1] For every 1000 kg of cement, the production process generates approximately 850 kg of carbon dioxide, which is released both as a by-product of chemical reactions and from the fossil fuels used by the kilns.[1] Replacing Portland cement with alternative binders such as alkali-activated binders (AABs) is one of the effective strategies to achieve the net zero carbon dioxide emission target.[2,3]

AABs are prepared using a precursor and an alkaline activator.[4] The most commonly used precursors include granulated blast furnace vitreous slags (GBFS), fly ash (FA) from coal combustion, and thermally activated metakaolin (MK).[5] Alkali-hydroxides and silicates, usually of sodium and potassium, are the most common alkaline activators[4] that can be added both in a liquid or a solid state.[4,6] Geopolymers (GPs) are a subset of AAB and are made from calcium-poor precursors (such as FA or MK) that give them a special chemical structure and specific chemical–physical and mechanical properties.[7,8]

AABs allow a significant reduction in carbon dioxide emissions compared to Portland cement due to their different chemical reactions and the absence of kiln firing.[4,9] For instance, the use of FA precursors produces only 250 kg of CO_2 per 1000 kg of binder.[8] Davidovits et al.[8] found a reduction of carbon dioxide emissions in the range of 75% to 90% using FA based cements when compared to Portland cement concrete. Additionally, the use of by-products as precursors enhances the environmental compatibility of the process.

Numerous studies have been conducted on alkali-activated and geopolymeric binders, while research on concretes made with these binders has primarily focused on material properties. A comprehensive review can be found in Davidovits[8] and Provis.[7] Many authors[4,10] have shown that the properties of these concretes vary significantly depending on the type of precursor used and the method of activation. While calcium-rich precursors result in the formation of $C-S-H$ gel and concrete-like properties, calcium-poor precursors result in the formation of GP three-dimensional chains that give the concrete unique chemical and physical properties that differ from those of OCs.[11]

Generally, AAB concrete can offer similar or even superior mechanical properties to Portland cement concrete, along with improved resistance to alkali-silica reaction and sulfate attack.[12–14] GPC, in particular, exhibits higher early strength, excellent chemical resistance, and low shrinkage and creep compared to traditional Portland cement concrete.[4,15,16] In addition, FA-based GPC shows better durability in aggressive environments, such as exposure to acids or sulfates,[4,17–19] and better fire resistance.[2,13,14]

From the mechanical point of view, AAB and GP concrete seem to be more brittle in compression.[20,21] Therefore, some authors suggest adding fibers to enhance ductility.[22,23] The Young modulus of the material is lower than that of Portland concrete, especially in the low to medium strength range.[11,24–26] For these reasons, the compressive stress–strain relationship of GPC shows some differences from that of Portland concrete[11] that can affect the mechanical behavior of structures.

In the field of civil engineering, understanding the behavior of structural elements is of paramount importance. Regarding the behavior of beams, studies have analyzed various factors influencing their behavior, including cracking moment, deformability, ultimate moment, shear strength, bond, and crack width. A review can be read in Mo et al.,[27] Ansari et al.,[20] and Dwibedy and Panigrahi.[28]

Regarding beams in flexure, the current literature reports mixed results. Some experimental studies have found that the behavior of beams in the elastic field is similar to that of Portland concrete beams,[21,27] with a cracking moment M_{cr} that may be equal or slightly higher.[27]

Lopes et al.[29] performed experimental four-point bending tests on small-scale beams reinforced with steel rebars. The authors compared the behavior of FA GPs with that of OC and observed that the former had a slightly lower modulus of elasticity, reduced maximum compressive strength, and lower values of ductility in terms of curvature.

Another study by Du et al.[30] performed four-point bending tests on FA GP beams and observed quite similar behavior to that of OC, except for higher deformability in the elastic field.

Alex et al.[31] also conducted bending tests on low-calcium FA-based GPC beams with steel bars to assess their bending behavior in terms of load-bearing capacity, deflection, crack propagation, and ultimate moment. Unlike Lopes et al.,[29] authors concluded that the GP beams exhibit higher ultimate loads and ductility than OC.

Upon analyzing experimental data, it can be observed that GPC beams exhibit similar behavior to Portland cement concrete beams in the elastic phase. However, in some cases, higher cracking moments have been noted. This behavior is consistent with studies on the material, which have shown that GPC can have a higher tensile strength than conventional concrete with the same compressive strength.[24,25,32–35] This effect is attributed to the nature of the chemical bonding, which results in a more homogeneous and less porous matrix than Portland cement concrete. As a result, the use of phenomenological equations for Portland cement concrete to estimate the flexural tensile strength of GPC beams based on the average compressive strength may not be appropriate.

When considering the ultimate moment M_u, the behavior of under-reinforced concrete beams, whose failure is controlled by the reinforcement, is similar to that of Portland cement beams.[21,35] However, in the case of over-reinforced beams, whose failure is controlled by the compressed concrete, a different behavior is observed.[21] In particular, concrete crushing occurs in a brittle, almost explosive manner. This difference is explained by the more brittle behavior of the material in compression. Some authors claim that the ultimate moment would be different from that of Portland concrete,[21] and, consequently, specific compression stress–strain relationships have been proposed to better understand the behavior of over-reinforced beams.[26,36]

While the principles of concrete design based on mechanics can be applied across different concrete types, applying standard concrete design codes to compute the cracking or the ultimate moment of GPC beams may not always yield accurate or reliable results. The unique properties and behavior of GPC must be taken into account to design structures, and specific standards must be used for this material.

Currently, no European standards exist for the design of GPC structures. The English code standard PAS 8820[37] refers to "Alkali-activated cementitious material and concrete", but it specifies only the performance requirements and the resulting concretes. Only the Australian SATS199[11] provides requirements for the design of AAB and GP building structures.

In the absence of a specific standard, some authors have considered using the ones for Portland concrete and have estimated the resulting model error.

Kathirvel et al.[38] performed a four-point bending test on GBFS reinforced concrete with recycled aggregates, finding that the ACI318[39] underestimates the ultimate moment. On the other hand, Zhang et al.[40] found the opposite result, both for cracking and ultimate moments from four-point bending tests on reinforced beams. Sumajouw et al.[35] observed that the AS3600 standard[41] tends to underestimate experimental results for low calcium FA-based GP-reinforced concrete beams both for cracking and ultimate moments. Ozturk et al.[42] made a comparison between their experimental data on GBFS concrete beams and the numerical cracking moment values obtained following different standard codes,[39,41,43,44] as well as some models for GPC beams.[25,45–49] Interestingly, he found that EC2:2004[43] and ACI318[39] overestimate the value of the cracking moment in contrast to the standards ACI363[44] and AS3600.[41] Additionally, Ozturk carried out the same procedure by comparing the experimental data and the theoretical values about the ultimate moment obtained following the ACI318 code,[39] finding relatively good but overestimated predictions. Worth noting, Ozturk's[42]

research is the only study currently available that considers EC2:2004 models for both cracking and ultimate moment.

Considering these results, it is important to compare the model error of multiple data. In fact, most researchers calculate the model error by referring to their experimental data without comparing it with other data obtained with different types of binder or amounts of reinforcement. By analyzing the model error for the different datasets, it will be possible to assess if the existing standard codes, although originally designed for Portland cement, are suitable for use in the flexural design of GPC beams.

To address this, the authors of the present article have collected extensive experimental data from the literature on the cracking and ultimate moment of GPC beams. The experimental data have been compared with analytical results obtained using the models of the main international standards for Portland cement concrete beams: 2nd generation EC2[50] (that from now on, it will be indicated as EC2), ACI318,[39] ACI363,[44] and AS3600.[41] The SATS199[11] standard, which is specific for GPC structures, was also considered. The experimental and analytical results have been compared to calculate the model errors. The binder types have been distinguished to ascertain their influence on the outcomes. In addition, to assess the importance of model errors, the same procedure was performed on an experimental data set for Portland cement concrete beams and compared with the results for GPs.

The work procedure is summarized and clarified as follows:

- Gathering of experimental data in terms of cracking moment $M_{cr,test}$ and ultimate moment $M_{u,test}$;
- Evaluation of M_{cr} and M_u according to EC2, ACI318, ACI363, SATS199, AS3600;
- Definition of three clusters by matrix type (GPC made with FA or GBFS, FA with SFs, OC);
- Evaluation of the model error for $M_{cr,test}/M_{cr}$ and $M_{u,test}/M_u$, and model quality indicators;
- Comparison and discussion of the models.

It is worth noting that in the literature, the term GP is usually, albeit improperly, used as a synonym for AAB.[4] Therefore, in the next part of this article, the term GP will be used without distinguishing between the two types of binders.

1.1 | Research significance

The spin-offs of the proposed work are multiple, both scientific and applicative. The first is to provide a contribution to the discussion for the development of specific

standards for GPC structures. In this area, the quantification of the model error is also useful for the definition of partial safety factors. Turning to the application aspects, it is noted that in some countries, the absence of specific standards requires that the design of GP structures, such as precast ones, goes through design by testing. The results of this work are useful for their pre-dimensioning.

2 | CRACKING MOMENT

The cracking moment M_{cr} is an important parameter in defining the serviceability behavior of reinforced concrete beams, as it governs the transition from the non-cracked state (stage I) to the cracked one (stage II). The cracking moment is usually defined as the value of the moment that causes the flexural tensile strength $f_{ctm,fl}$ (also known as modulus of rupture) to be reached in the extreme tension fiber, that is,

$$M_{cr} = \frac{f_{ctm,fl} \cdot I_{om}}{y_t} \qquad (1)$$

where I_{om} is the moment of inertia of the homogenized section and y_t is the distance of the extreme tension fiber from the centroid of the homogenized section. Typically, standards define the value of the mean flexural tensile strength $f_{ctm,fl}$ as a function of the compressive strength of the concrete using phenomenological formulae. For example, EC2[50] calculates the flexural tensile strength $f_{ctm,fl}$ as a function of the mean tensile strength f_{ctm} of concrete and the beam height h, which accounts for the so-called size effect:

$$f_{ctm,fl} = \max\left[\left(1.6 - \frac{h}{1000}\right)f_{ctm}; f_{ctm}\right] \qquad (2)$$

The average tensile strength f_{ctm} is expressed by the EC2[50] as

$$f_{ctm} = \begin{cases} 0.3 f_{ck}^{2/3} & f_{ck} \leq 50\,\text{MPa} \\ 1.1 f_{ck}^{1/3} & f_{ck} > 50\,\text{MPa} \end{cases} \qquad (3)$$

where f_{ck} is the characteristic compressive strength of concrete.

According to the EC2,[50] $f_{ck} = f_{cm} - 8$ MPa, in agreement with Rüsch.[51] This simple relationship between f_{ck} and f_{cm} was confirmed in several experimental campaigns, where mean strength and standard deviation were measured.[52]

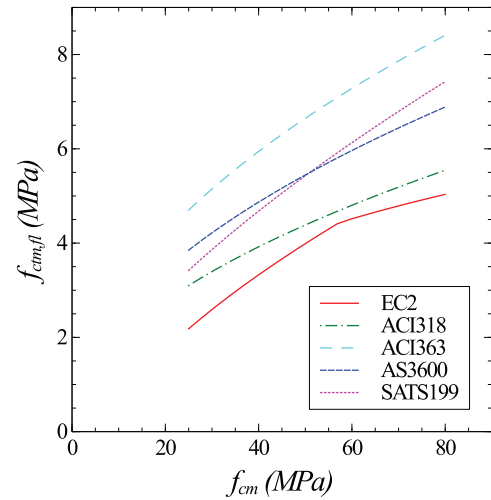The American code ACI318[39] for normal weight concrete, suggests calculating

FIGURE 1 Mean flexural tensile strength $f_{ctm,fl}$ as a function of mean compressive strength f_{cm} according to some code standards.

$$f_{ctm,fl} = 0.62\lambda\sqrt{f_c'} \qquad (4)$$

in which the coefficient λ is equal to 1 for normal weight concrete and f_c' is the specified compressive strength. Since Equation 4 was calibrated on the basis of experimental results, according to Nowak et al.,[53] for comparisons with experimental data, the value f_c' can be replaced with the average compressive strength f_{cm}.

The ACI363 code[39] for high strength concrete provides

$$f_{ctm,fl} = 0.94\sqrt{f_c'} \quad 21\,\text{MPa} < f_c' < 83\,\text{MPa} \qquad (5)$$

The Australian code AS3600[41] adopts the relationship:

$$f_{ctm,fl} = 0.77\sqrt{f_{cm}} \qquad (6)$$

Finally, the Australian SATS199 code,[11] which is specific for geopolymeric concretes, gives the following equation

$$f_{ctm,fl} = 0.4(f_{cm})^{2/3} \qquad (7)$$

As can be seen, the different equations vary significantly from each other. However, to facilitate comparisons, the flexural strengths $f_{ctm,fl}$ have been plotted in Figure 1 as a function of the mean compressive strength f_{cm}. For consistency, a beam with a height $h = 500$ mm was assumed, and the different compressive strengths were related to the average strength f_{cm} as described

TABLE 1 Summary of experimental data for cracking moment in GPC and OC beams.

No.	Reference	N. of data.	Type of binder	b (mm)	h (mm)	f_{cm} (MPa)	ρ (%)
1	Sumajouw et al.[35]	12	FA	200	300	37–76	0.62–2.47
2	Shibayama et al.[54]	6	FA	150	250	29.9–50.1	0.73
3	Ozturk et al.[42]	6	GBFS	150	240	46.18–71.0	1.28
4	Maranan et al.[55]	1	GBFS	200	300	31	1.18
5	El-Sayed[56]	2	FA	150	300	66.3–114.9	0.25–0.4
6	Alex et al.[31]	3	FA	125	250	22.8–24.1	0.55
7	Zhang et al.[40]	7	FA	95–102	238–255	37.6–41.1	0.65–2.12
8	Saranya et al.[36]	1	FA	100	150	54.67	1.21
9	Mathew et al.[57]	5	FA	150	200	25.58–47.46	0.58
10	Mudimby et al.[58]	18	FA, GBFS	100	155	30.65–62.33	0.19–2.49
11	Jeyasehar et al.[59]	4	FA	125	250	35.64–37.39	0.90
12	Bosco et al.[60]	18	OC	100	100–400	75.96	0–0.31
13	Fantilli et al.[61]	2	OC	200	500	41.3	0.22
14	Pecce et al.[62]	6	OC	400	180	41.3–95.4	1.09–2.59
15	Fantilli et al.[63]	1	OC	100	150	40.42	0
16	Fantilli et al.[64]	2	OC	150	282	51.4	2.32
17	Yacob et al.[65]	1	OC	203	305	43.4	1.57
18	Lopes et al.[29]	3	OC	100	150	29.05	0.4–0.81
19	Jang et al.[66]	16	OC	140	245–260	40–75	1.37–5.57
21	Zhang et al.[40]	4	OC	125	250	25.4–50,6	0.55
22	Saranya et al.[36]	2	OC	100–105	250–258	43.2–47.9	1.21–1.31

earlier. It is notable that the curves ACI318[39] and EC2[50] are closer to each other, whereas the ACI363[44] curve provides the highest resistance values.

Experimental data were collected from the literature to understand how these equations behave in the case of GPC. More specifically, 65 GPC (13 made with GBFS and 52 with FA) were collected from published references. Table 1 contains the references, the number of specimens N, the type of binder, the base b and height h of the beam, the mean compressive strength f_{cm}, and the geometric reinforcement ratio $\rho = A_s/(bh)$, where A_s is the area of the reinforcement in tension.

The range of compressive strengths f_{cm} varies between 23 and 115 MPa, with heights h between 150 and 300 mm and the geometric reinforcement ratio ρ between 0.19% and 2.49% (Table 1). Starting from the experimental data, the experimental flexural strength $f_{ctm,fl}$ was obtained from Equation (1) as

$$f_{ctm,fl} = \frac{M_{cr,test} \cdot y_t}{I_{om}} \quad (8)$$

Figure 2a shows the experimental values $f_{ctm,fl}$ as a function of f_{cm}. The figure reveals that for $f_{cm} > 50$ MPa

the scatter of $f_{ctm,fl}$ is higher, especially for GBFS samples. In addition, a change in the slope of the trend of the experimental points is evident for FA samples. For each sample, the corresponding analytical value of M_{cr} was computed using Equations (2–7) for different standards.[11,39,41,44,50] The ratio between the experimental value $M_{cr,test}$ and the analytical value M_{cr} gave the model error, which is shown in Figure 3a–e. In the same figures, the horizontal line represents the mean value μ_θ of the error.

EC2[50] (Figure 3a) gives the best results for GPC, with errors between 0.64 and 1.30 and a mean value $\mu_\theta = 0.97$. It can be noticed that the dispersion of data is higher for FA with low f_{cm} whereas in the case of GBFS, the dispersion increases with high strengths. The greater uncertainties for the GBFS than for FA specimens are also confirmed by the ACI318[39] model in Figure 3b. In this case, the mean error is $\mu_\theta = 1.03$. Figure 3c shows the results for the ACI363[44] model, which gives values that are less than unity, with a mean error $\mu_\theta = 0.68$; the model, therefore, significantly overestimates the cracking moment. Finally, Figure 3d shows the results for the models AS3600[41] and Figure 3e for SATS199.[11] The mean values of the errors are $\mu_\theta = 0.85$ and $\mu_\theta = 0.83$,
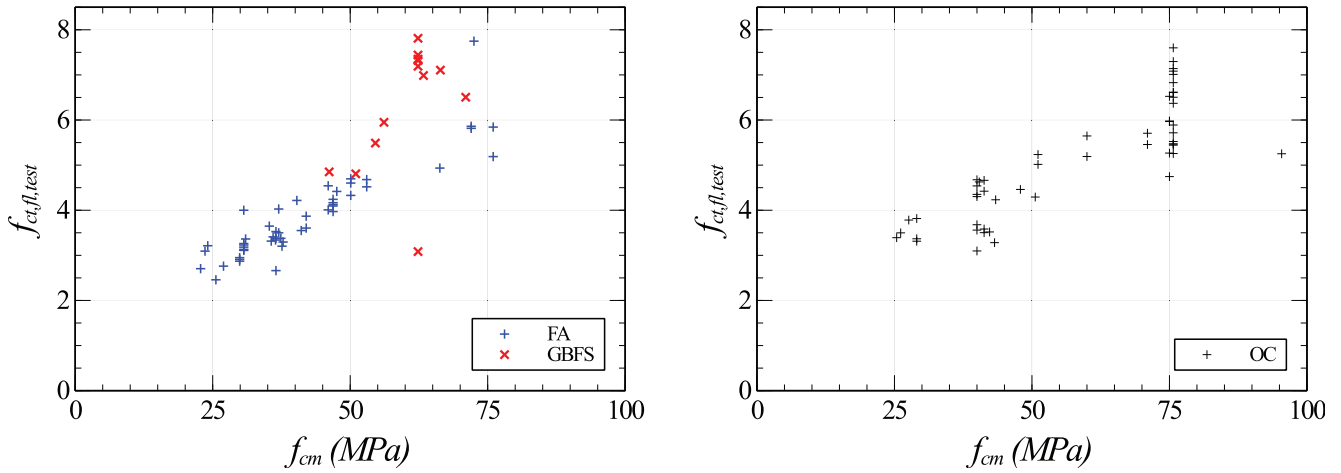
FIGURE 2 Variation of the experimental flexural strength $f_{ct,fl,test}$ as a function of f_{cm}: A) GPC; b) OC.
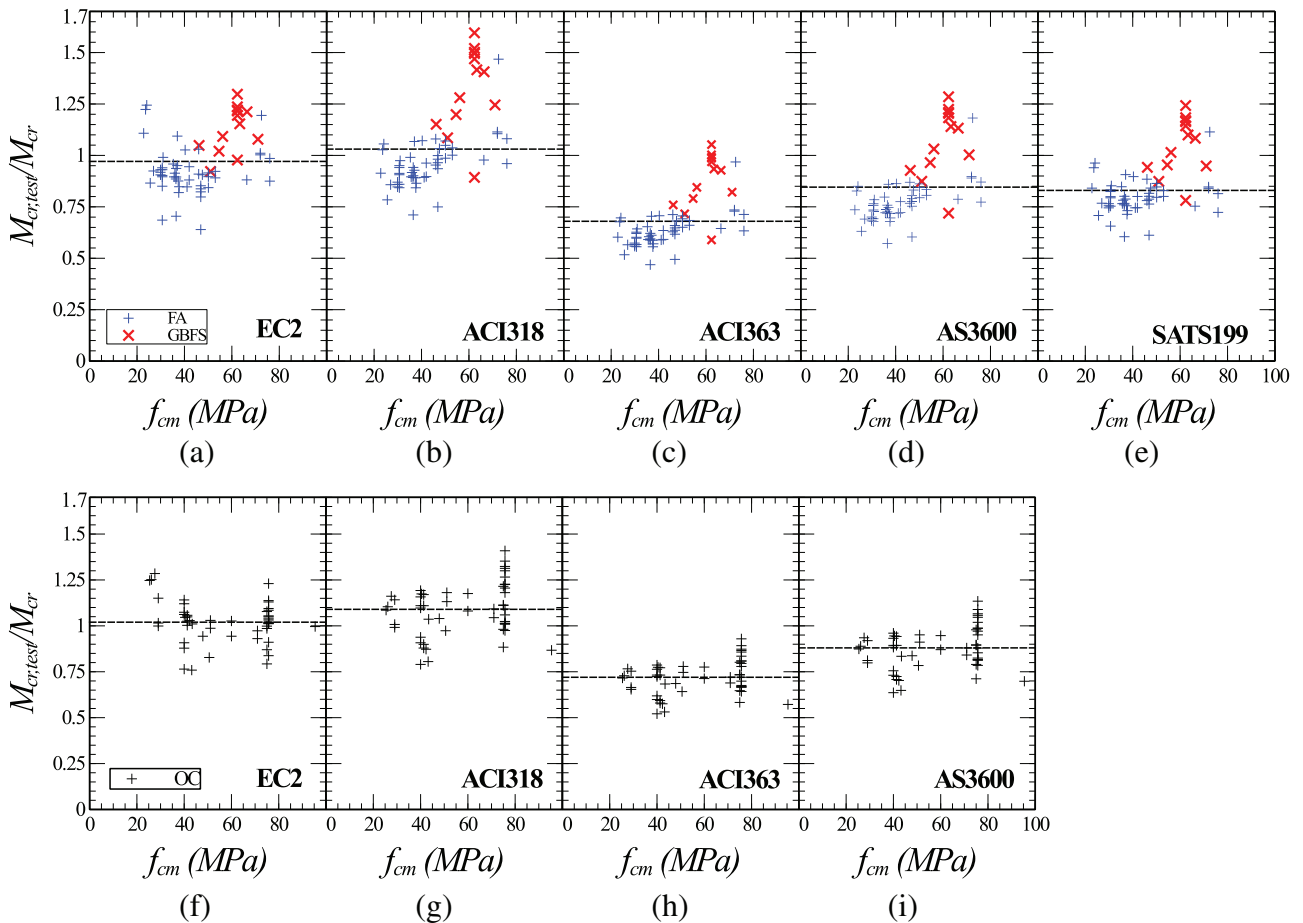

FIGURE 3 Comparing the model error for the cracking moment $M_{cr,test}/M_{cr}$ as a function of f_{cm} considering the models of various standards and evaluated for GPC and OC. The considered standard models are: The EC2,[50] the ACI318,[39] the ACI363,[44] the AS3600,[41] and the SATS199.[11] In particular, for GPC, the results are reported in (a–e), while for OC are shown in (f–i).

respectively. Furthermore, it can be observed that in all models, the GBFS points show errors greater than the mean value. To compare the different models, the

minimum *min*, maximum *max*, and mean μ_θ values of the errors and the corresponding coefficient of variation (COV) are summarized in Table 2. The same table shows

TABLE 2 Model error $M_{cr,test}/M_{cr}$ for GPC and OC beams using different standard codes: Minimum min; maximum max; mean value μ_θ; coefficient of variation, COV; and percentage of specimens with error smaller than 20% i_{20}.

Model	GPC					OC				
	min (−)	max (−)	μ_θ (−)	COV (−)	i_{20} (%)	min (−)	max (−)	μ_θ (−)	COV (−)	i_{20} (%)
EC2[50]	0.64	1.30	0.97	0.15	82.82	0.76	1.28	1.02	0.11	85.8
ACI318[39]	0.71	1.60	1.03	0.20	77.62	0.79	1.41	1.09	0.13	70.9
ACI363[44]	0.47	1.05	0.68	0.20	22.63	0.52	0.93	0.72	0.13	26.2
SATS199[11]	0.57	1.29	0.83	0.20	42.64	-	-	-	-	-
AS3600[41]	0.60	1.24	0.85	0.16	61.85	0.64	1.13	0.88	0.13	85.9

the parameter i_{20}, which expresses the percentage of points evaluated with an error of less than 20%. This parameter is less sensitive to outliers and can be conveniently used to compare models.[67] The results indicate that the SATS199[11] model, although proposed for GPC, produces greater errors for the examined cases than those of EC2[50] and ACI318[39] codes. The errors for these two models are relatively small.

To limit shrinkage cracking, fibers can be added to the GPC matrix. However, the existing literature on the experimental cracking moment of fiber-reinforced GPC often lacks essential informations about the fibers used (in terms of diameter, length, shape, percentage, strength, etc.), which are necessary for calculating the cracking moment according to the standard codes. Therefore, fiber-reinforced GPs will not be included in the present study. Similarly, regarding the mix design, it was not possible to differentiate the potential influence of the various factors due to the insufficient quantity of data and the absence of detailed mix design information in many studies.

The procedure previously described was applied to an experimental dataset of OC beams to determine if the model errors were greater than those of Portland cement concrete. A summary of the experimental data is reported in Table 1. The range of compressive strengths f_{cm} varied between 25 and 95 MPa, the beam height h between 100 and 500 mm and the geometric reinforcement ratio ρ between 0% and 5.57% (Table 1). In Figure 2b, the trend of the experimental values of flexural strength $f_{ctm,fl}$ as a function of the compressive strength f_{cm} is shown. The dispersion of points is rather wide, especially for data belonging to a specific experimental campaign[60] with compressive strength equal to 75.96 MPa.

For each sample, the corresponding analytical value of M_{cr} was calculated using the formulae provided by EC2,[50] ACI318,[39] ACI363,[44] and AS3600.[41] The ratios between the experimental cracking moments $M_{cr,test}$ and the analytical ones M_{cr} are shown in Figure 3f–i.

Also in this case, the EC2[50] model (Figure 3f) gave the best results with $\mu_\theta = 1.02$, despite a significant dispersion of the points for low f_{cm}. In this region, EC2[50] tends to underestimate the experimental values. Figure 3g shows that the ACI318[39] model gave ratios slightly greater than one ($\mu_\theta = 1.09$). In contrast, the ACI363 (Figure 3h) and AS3600 (Figure 3i) models gave ratios whose mean values were less than one, that is, they tend to underestimate the cracking moment. Furthermore, the results are summarized in Table 2. A comparison of the results obtained for the GPC and OC beams reveals that the model errors are similar, both as mean value and COV. Regarding the effects of shrinkage, it is known that in concrete it generates tensile self-tensions that affect the cracking moment.[68] However, in GPC, the literature offers contradictory findings regarding the effects of drying shrinkage on its cracking performances, depending on the mix design, curing method, and specimen size[4,16,69]; therefore, this aspect is not considered in the study.

3 | ULTIMATE BENDING MOMENT

One of the fundamental aspects of designing reinforced concrete beams is calculating the ultimate moment M_u. Figure 4 shows the calculating sequence adopted by the main standards. It is possible to observe the cross-section of the beam, the plane strain diagram, the stress distribution for concrete and steel, and the resulting forces. In particular, C_c is the force in the compressed concrete, C_s' is the force in the compressed steel, T_s is the force in the tension steel, and T_c is the force in the tension concrete if fibers are present.

The position x of the neutral axis $n-n$ is computed by solving the non linear equilibrium equation

$$C_c + C_s' - T_s - T_c = 0 \qquad (9)$$

Then, M_u is obtained from the rotational equilibrium equation of the four forces with respect to $n-n$
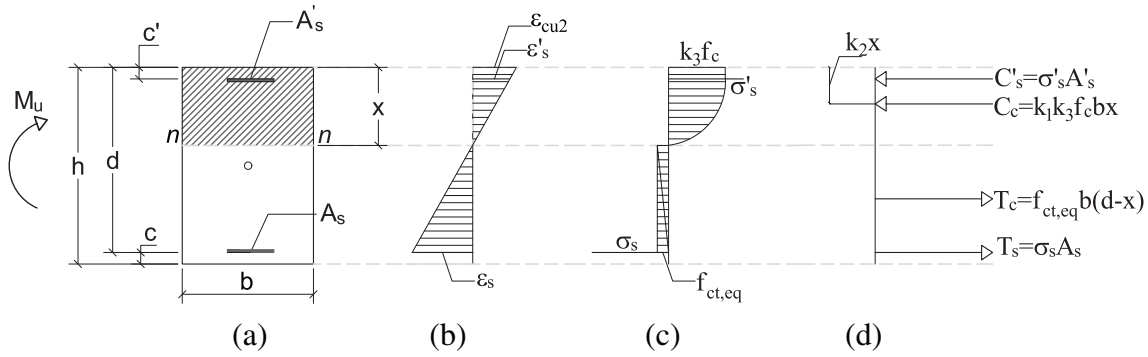
FIGURE 4 Determination of the ultimate moment M_u: (a) beam cross-section; (b) strain profiles; (c) stresses; (d) resultants.

$$M_u = C_c x(1 - k_2) + C_s'(x - c') + T_s(d - x) + T_c(d - x)/2 \tag{10}$$

where

$$C_c = k_1 k_3 f_c b x \tag{11a}$$

$$C_s' = \sigma_s' A_s' \tag{11b}$$

$$T_s = \sigma_s A_s \tag{11c}$$

$$T_c = f_{ct,eq} b(d - x)/2 \tag{11d}$$

in which the coefficients k_1, k_2, and k_3 depend on the adopted constitutive law for compressed concrete. More in detail, k_1 is the ratio between the average compressive stress to the maximum stress

$$k_1 = \frac{\int_0^x \sigma_c b d\xi}{b x f_c} \tag{12}$$

k_2 is the ratio between the distance of C_c from the extreme compression fiber to the depth of the neutral axis x

$$k_2 = 1 - \frac{\int_0^x \sigma_c \xi b d\xi}{b \int_0^x \sigma_c b d\xi} \tag{13}$$

and k_3 is the ratio between the maximum concrete stress to the concrete strength f_c. The definition of f_c varies in the considered standards and will be specified later. Table 3 summarizes the expressions of k_1, k_2, and k_3 according to EC2,[50] ACI318,[39] AS3600,[41] and SATS199[11] codes.

To determine the coefficients, the EC2[50] assumes that the compressive stress–strain relationship for concrete is given by the equation:

$$\sigma_c = \begin{cases} k_3 f_c \left[1 - \left(1 - \frac{\epsilon_c}{\epsilon_{c2}} \right)^2 \right] & 0 \leq \epsilon_c \leq \epsilon_{c2} \\ k_3 f_c & \epsilon_{c2} \leq \epsilon_c \leq \epsilon_{cu2} \end{cases} \tag{14}$$

in which $\epsilon_{c2} = 2‰$ and $\epsilon_{cu2} = 3.5‰$, regardless of concrete compressive strength f_c.

The values of k_1 and k_2, which are obtained by integration of the stress–strain relationship, are reported in Table 3. The same table shows the value of k_3 that depends on the characteristic compressive strength of concrete f_{ck}, the reference strength $f_{ck,ref} = 40$ MPa, and $k_{tc} = 1$ for short term loading.

The American code ACI318[39] assumes that concrete stress $k_3 f_c$ is uniformly distributed over an equivalent rectangular stress-block bounded by the top edge of the cross-section and a line parallel to the neutral axis and located at a distance $k_1 x$ from the top edge.

The coefficient k_1 varies between 0.65 and 0.85 as a function of the specified compressive strength f_c' (Table 3). ACI318[39] assumes $k_3 = 0.85$ observing that a large variation in compressive strength of concrete does not cause a significant change in the flexural capacity of the section. The ultimate strain ϵ_{cu2} is fixed at 3‰.

The Australian code AS3600[41] considers a linear variation of k_3 with f_c'. Similarly to the ACI318,[39] the stress-block is rectangular but with a coefficient k_1 that is a linear function of f_c' (Table 3).

The Australian code SATS199[11] assumes that the stress–strain relationship of GPC is formed by a first linear branch for $\epsilon < \epsilon_{c2}$ followed by a constant branch for $\epsilon_{c2} \leq \epsilon < \epsilon_{cu2}$ with:

TABLE 3 Expressions of the coefficients k_1, k_2, and k_3 according to the considered code standards.

Model	k_1		k_2	k_3
EC2[50]	0.8095		0.4160	$k_{tc}\min\left[\left(\frac{f_{ck,ref}}{f_{ck}}\right)^{1/3},1\right]$
ACI318[39]/ACI363[44]	$\begin{cases} 0.85 & f'_c < 27.6 \text{ MPa} \\ 0.85-0.05\frac{145.05f'_c-4000}{1000} & 27.6 \text{ MPa} \le f'_c < 55.16 \text{ MPa} \\ 0.65 & f'_c \ge 55.16 \text{ MPa} \end{cases}$		$0.5k_1$	0.85
AS3600[41]	$0.97-2.5\cdot10^{-3}f'_c$		$0.5k_1$	$0.85-0.0015f'_c$
SATS199[11]	$1-\frac{\epsilon_{c2}}{2\epsilon_{cu2}}$		$\frac{\epsilon_{c2}^2-3\epsilon_{c2}\epsilon_{cu2}+9\epsilon_{cu2}^2}{3\epsilon_{cu2}(-\epsilon_{c2}+2\epsilon_{cu2})}$	$0.85-0.0015f'_c$
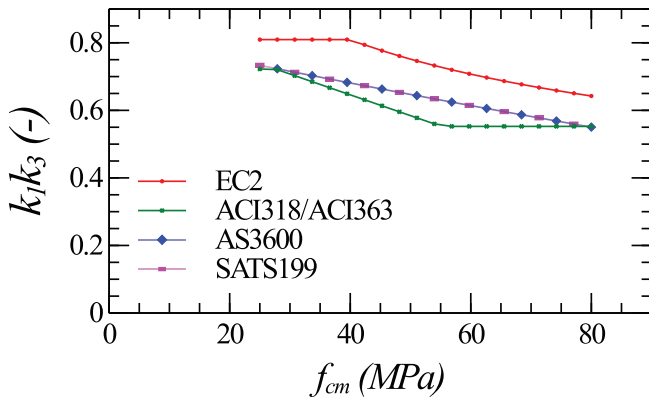
FIGURE 5 Comparison of different standards for calculating the ultimate moment of RC beams: Product of the coefficients k_1 and k_3 as a function of f_{cm}.

$$\epsilon_{c2} = 1.21\alpha_2 \cdot \frac{f'_c}{E_{cj}} \qquad (15)$$

$$\epsilon_{cu2} = \frac{1.14f'_c}{k_E \cdot E_{cj}} \ge 0.003 \qquad (16)$$

where

$$E_{cj} = \begin{cases} 5050\sqrt{f_{cm,j}} & f_{cm,j} \le 40 \text{ MPa} \\ 14100+2820\sqrt{f_{cm,j}} & f_{cm,j} > 40 \text{ MPa} \end{cases} \qquad (17)$$

and $k_E = 0.14+0.012f'_c$ with $0.5 \le k_E \le 0.74$, and $\alpha_2 = k_3$. The values of k_1 and k_2 are obtained by integration of the stress–strain relationship. The expressions of the coefficients are reported in Table 3.

A comparison of the product k_1k_2, which rules compressive force in concrete C_c, is shown in Figure 5 for the different standards previously described. To allow comparison with the experimental data, the value f_{cm} was used instead of f_c, f_{ck}, $f_{cm,j}$, and f'_c in the previous equations. It is possible to observe a noticeable difference in k_1k_2 between the standards. In particular, EC2[50] gives the highest values while ACI318[39] gives the lowest.

Regarding the stress–strain relationship of reinforcing bars, the EC2[50] assumes a linear elastic branch up to the yield stress f_y, followed by a linear hardening branch up to the failure stress f_t, which corresponds to the ultimate strain ϵ_u. In contrast, the other standards analyzed here assume a perfectly plastic behavior after yielding.

Frequently, GPC are fiber-reinforced to increase the shear strength, reduce the crack width, and improve ductility in compression. For this reason, this study also considers fiber-reinforced GP beams.

In this context, the concrete tensile strength contribution T_c (Equation 11d) is taken into account in Equations (9) and (10). The standards considered do not cover the use of fibers. According to Model Code 2010,[70] the value of T_c depends on the equivalent tensile strength of concrete $f_{ct,eq}$. In the case of work hardening or degrading bending behavior of the experimental tensile stress-crack width curves, equivalence formulae are given to obtain the equivalent tensile strength $f_{ct,eq}$. The American standard ACI544.4R-11[71] also provides guidelines for fiber-reinforced concrete beams. However, it requires information on fibers (such as diameter, length, and tensile strength) that are not always available in the experimental references.

In order to ascertain the suitability of the described code standard models for GPC, experimental data were gathered from the literature. For comparative purposes, data were collected for GPC beams with and without fibers and for Portland cement concrete beams. Table 4 summarizes the data for GPC with and without SFs and for OC. The table includes the references, the number of specimens, the type of binder, the base b, and the height h of the beams, the mean compressive strength of concrete f_{cm}, the geometric reinforcement ratio $\rho = A_s/(bd)$ where A_s is the area of the reinforcement in tension, and the mechanical reinforcement ratio $\omega_s = A_sf_y/(bdf_{cm})$.

TABLE 4 Summary of experimental data on ultimate moment M_u of GPC, with and without SFs, and OC beams.

No.	Reference	N. of data	Type of binder	b (mm)	h (mm)	f_{cm} (MPa)	ρ (%)	ω_s (%)
1	Sumajouw et al.[35]	12	FA	200	300	37–76	0.6–2.5	4.5–37.2
2	Shibayama et al.[54]	6	FA	150	250	30–59	0.7	5.3–8.8
3	Ozturk et al.[42]	6	GBFS	150	240	46.2–71.0	1.3	11.5–16.5
4	Maranan et al.[55]	1	GBFS	200	300	31	1.2	19.0
5	Kathrivel et al.[38]	3	GBFS + FA	150	150	33.4–35.4	1.9	28.1–33.5
6	Lopes et al.[29]	2	FA	203	305	41.2–43.4	1.57	20.3–28.1
7	Kumar et al.[72]	5	GBFS	100	150	19.8	0.4–1.4	11.7–44.6
8	Tauquir et al.[73]	2	FA	150	225	36.9	2.1	25.6
9	Yacob et al.[65]	5	GBFS	100	150	49.7–55.9	1.8	18–18.9
10	Lin et al.[74]	6	GBFS+FA	150	300	33.1	0.24–2.99	3.96–49.99
11	Bayuaji et al.[75]	6	FA	100	150	14	0.77	12.94–13.25
12	Yost et al.[21]	6	FA	305	152	52.2–54.7	1.56–4.91	12.35–38.92
13	Cong et al.[76]	3	FA	200	300	35	1.16–2.82	15.52–37.49
14	Hammad et al.[77]	1	FA	100	200	40.5	1.32	14.08
15	Yacob et al.[65]	1	OC	203	305	43.4	1.6	20.3
16	Kathirivel et al.[38]	1	OC	100	150	40	1.8	23.4
17	Lopes et al.[29]	5	OC	100	150	29.1	0.4–1.4	8–30.4
18	Mansur et al.[78]	2	OC	170	250	72.9–76.3	6.3	45.6–47.8
19	Alca et al.[79]	3	OC	150–335	282–630	51.4–54.2	2.3–2.4	17.5–18.1
20	Ulfkjaer[80]	2	OC	100–200	200–400	22.8–24.8	1.7–8.2	44.7
21	Ko et al.[81]	35	OC	150–200	150–180	66.6–82.1	1.6–6.5	11.1–34.5
22	Jang et al.[66]	19	OC	140	195–210	40–75	1.9–5.6	11.8–45.2
23	Su et al.[82]	5	SF	150	300	145.6–156.2	1.10–2.24	3.53–6.78
24	Tran et al.[83]	4	SF	150	200	61–70	0.7	5.3–6.1
25	Ozturk et al.[42]	5	SF	150	240	51–71	1.3	10.7–14.9
26	Kathirvel et al.[38]	5	SF	150	150	49.5–55.9	1.77	16.8–18.9
27	Monfardini et al.[84]	5	SF	200	460	24–37	0.5	7–11
28	Yacob et al.[65]	2	SF	203	305	41.2–43.4	1.6	6.9–10.7
29	Monfardini et al.[85]	2	SF	200	300	33.2–37.5	0.77	20.3–21.4

More specifically, 64 GPC (26 made with GBFS and 38 with FA), 68 OC, and 28 GPC fiber reinforced test results were collected.

Concerning the GPC samples, the range of compressive strength f_{cm} varies between 14 and 76 MPa with heights h between 150 mm and 305 mm and geometric reinforcement ratio ρ between 0.24% and 4.91% (Table 4).

Figure 6a shows the experimental values in terms of the dimensionless ultimate moment $\mu_u = M_{u,test}/(bd^2 f_{cm})$ as a function of mechanical reinforcement ratio ω_s. Figure 6a shows that for $\omega_s > 0.25$, the scatter of μ_u is higher, especially for the GBFS samples.

For each sample, the corresponding analytical value of M_u was computed using the equations for the five standards considered. The ratio between the experimental ultimate moment $M_{u,test}$ and the analytical ultimate moment M_u provided the model error, which is shown in Figure 7a–d. In particular, the markers represent the analyzed experimental points while the horizontal lines show the mean error μ_θ. The mean errors μ_θ and the corresponding COV are summarized in Table 5. The same table shows the parameter i_{20} and the minimum and maximum values of the error.

EC2[50] (Figure 7a) gave the best results for GPC, with ratios between 0.92 and 1.16 and a mean error $\mu_\theta = 1.06$. It can be noticed that EC2 model is suitable both for FA and GBFS samples regardless of the value of ω_s with a high value of $i_{20} = 94.64$. Greater uncertainties are
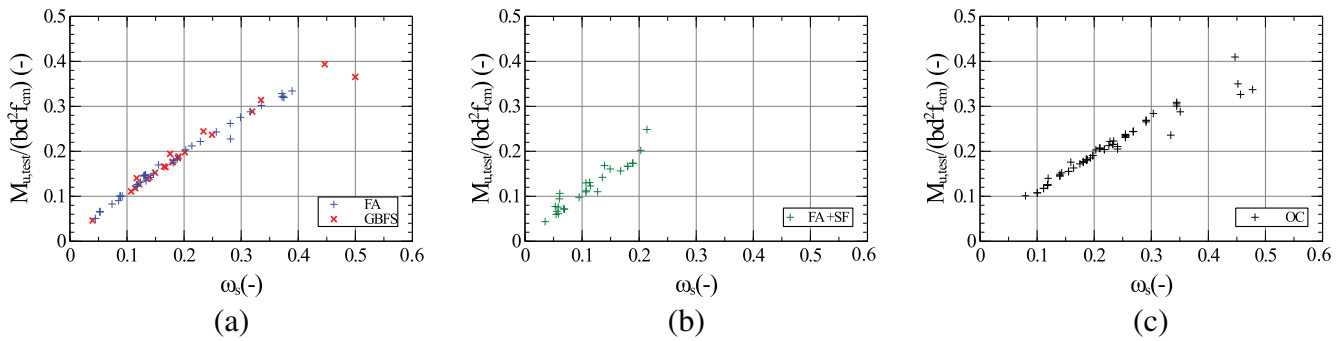
FIGURE 6 Experimental dimensionless ultimate moment μ_u as a function of mechanical reinforcement ratio ω_s, results for beams in: A) GPC with FA or GBFS precursors; b) GPC with SFs; c) OC.

observed by the ACI318[39] model (Figure 7b). In this case, the mean error is $\mu_\theta = 1.25$. The model, therefore, underestimates the experimental value of the ultimate moment. Finally, Figure 7c shows the results for the models of the AS3600[41] and Figure 7d for SATS199[11] standards. The mean errors are $\mu_\theta = 1.14$ and $\mu_\theta = 1.09$, respectively. In the examined cases, the results demonstrate that the SATS199,[11] despite being proposed for GPC, produces greater errors than EC2[50] but better than AS3600.[41] The errors for these two models are relatively small when compared to the ACI318[39] results. In addition, it can be seen that for all models, the error tends to be almost constant both for low and high values of ω_s, that is, for the less and most heavily reinforced beams.

The same procedure was followed for fiber-reinforced FA + SF samples. Table 4 shows a summary of the data. The range of compressive strengths f_{cm} varies between 24 MPa and 156.2 MPa with beam height h between 150 mm and 460 mm and geometric reinforcement ratio ρ between 0.7% and 2.24% (Table 4). In this case, since the articles considered did not provide the tensile stress–strain curve of the fiber concrete or the properties of the fibers, but only the cracking moment of the beam, it was assumed that $f_{ct,eq}$ was equal to $f_{ct,fl}$, thus overestimating its value. Figure 6b shows the experimental values of μ_u as a function of ω_s. It is possible to observe that the trend of μ_u is approximately linear with ω_s.

Also in this case, for each sample, the corresponding analytical value of M_u was computed using the equations for the considered standards.[11,39,41,44,50] The ratio between the experimental value $M_{u,test}$ and the analytical value M_u provided the model error, which is shown in Figure 7d–f and summarized in Table 5 with also the minimum *min*, maximum *max* values of the errors, the corresponding coefficients of variation COV, and the parameter i_{20}.

Similarly to previous results, the EC2[50] model (Figure 7e) gave the lower uncertainties with ratios

between 0.74 and 1.20 and a mean value of $\mu_\theta = 0.99$ (Table 5). Similar results were obtained for the AS3600[41] (Figure 7g) and SATS199[11] models (Figure 7h) with lower mean values of 0.91 and 0.89, respectively (Table 5). In contrast, the ACI318[39] model shown in Figure 7f underestimated the experimental moments with a mean of $\mu_\theta = 1.02$ (Table 5). Looking at the results, it seems that models that tend to overestimate the resistant moments gave better results in the presence of fibers. In any case, it seems that in the case of concretes reinforced with fibers, it is necessary to evaluate the contribution of fibers with precision.

Furthermore, to determine whether the model error in the ultimate moment for GPC beams is greater than that for Portland cement, the same procedure was applied to an OC experimental data set. A summary of the experimental data is given in Table 4. The range of compressive strengths f_{cm} was between 29.1 and 82.1 MPa for specimens with heights h between 150 and 650 mm and a geometric reinforcement ratio ρ between 0.4% and 8.2% (Table 4). An essentially linear relationship between the data is observed by Figure 6c, which displays the experimental values μ_u as a function of ω_s, although a slight change in the slope of the trend of the experimental points is observed at $\omega_s = 0.25$.

For each sample, the corresponding analytical value of M_u was also computed using the formulae provided by EC2,[50] ACI318,[39] ACI363,[44] and AS3600.[41] The model SATS199[11] was not used because it is specific for GPC. The ratios between the experimental values $M_{u,test}$ and the analytical ones M_u provided the model errors, which are shown in Figure 7i,l,m, while Table 5 summarizes the other parameters.

Again, the EC2[50] (Figure 7i) gave the best results with ratios between 0.79 and 1.10 and a mean of $\mu_\theta = 1.00$ (Table 5). Different results were obtained for the AS3600 (Figure 7m). In this case, the mean error is $\mu_\theta = 1.11$ (Table 5). Finally, Figure 7l shows the results for the models of the ACI318[39] standard. The mean error is 1.24
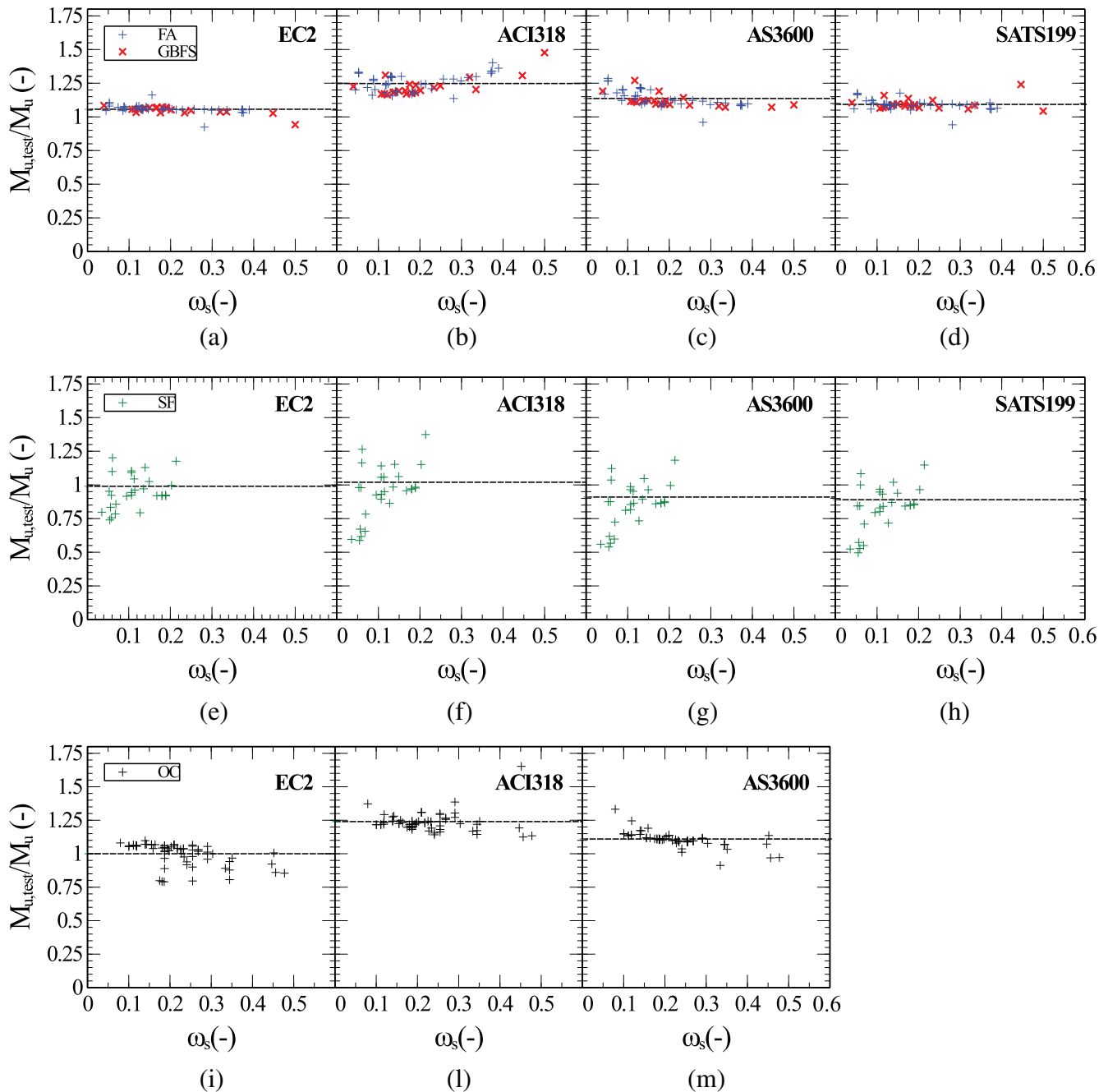
FIGURE 7 Model error for ultimate moment $M_{u,test}/M_u$ as a function of mechanical reinforcement ratio ω_s using different codes[11,39,41,50]; (a)–(d) GPC both precursed with FAs or GBFS; (e)–(h) GPC with fibers (SF); (i)–(m) OC.

(Table 5). The results indicate that the ACI318[39] model produces more significant errors for the cases studied than those produced by the EC2[50] and also AS3600[41] models. The errors for the EC2[50] model are relatively small, confirming again, the EC2[50] gave the best results.

An examination of Table 5 reveals that, when using the same model, the outcomes between GPC and OC are strikingly similar, both in terms of the mean value, μ_θ, and the COV. Consequently, it appears feasible to employ these models for estimating the ultimate moment in the context of GPC. However, it is important to note that the limited availability of experimental data for heavily reinforced beams raises some concerns and prevents definitive conclusions from being drawn. The discrepancy between the various standards is not unexpected, given the differing regulatory frameworks. Additionally, it is common to encounter a significant degree of uncertainty in all the cases examined, which can be attributed to the fact that some experimental campaigns do not report data with the required accuracy.

TABLE 5 Model error $M_{u,test}/M_u$ for GPC, SF and OC beams using different standard codes: Minimum *min*; maximum *max*; mean value μ_θ; coefficient of variation, COV; and percentage of specimens with error smaller than 20% i_{20}.

Model	GPC					SF					OC				
	min (−)	*max* (−)	μ_θ (−)	COV (−)	i_{20} (%)	*min* (−)	*max* (−)	μ_θ (−)	COV (−)	i_{20} (%)	*min* (−)	*max* (−)	μ_θ (−)	COV (−)	i_{20} (%)
EC2[50]	0.92	1.16	1.06	0.03	94.64	0.74	1.20	0.99	0.105	92.45	0.79	1.10	1.00	0.082	93.99
ACI318[39]	1.14	1.48	1.25	0.068	27.56	0.59	1.37	1.02	0.131	84.84	1.12	1.65	1.24	0.058	17.83
SATS199[11]	0.94	1.24	1.09	0.040	90.08	0.50	1.15	0.89	0.120	97.53	-	-	-	-	-
AS3600[41]	0.96	1.29	1.14	0.059	70.10	0.54	1.18	0.91	0.122	99.82	0.50	1.15	0.89	0.122	87.66

4 | CONCLUSIONS

In this study, the authors collected from the literature the experimental cracking moment M_{cr} and ultimate moment M_u data of GPC beams reinforced with steel bars, both made with FA and GBFS. The cluster category exhibits considerable diversity with respect to mixture design and production methods. This variability depends on the fact that the use of GP cement in structural engineering applications is relatively new and, consequently, there is still a lack of available comprehensive data in the literature; the authors have compared design specifications despite the numerous disparities, with the aim of obtaining a sufficient data set for meaningful comparisons. The gathered experimental tests were assessed using different standard codes: 2nd generation EC2,[50] ACI318,[39] ACI363,[44] AS3600,[41] and SATS199,[11] which is specific for GPC. The model errors were evaluated for the different data sets. To investigate whether and how the model error was larger than that for OC, the same procedure was repeated on reinforced concrete beams made with Portland cement. The results suggest the following conclusions:

- Considering the experimental flexural strengths $f_{ct,fl}$, it can be observed that the dispersion of data in the FA case was greater for low values of f_{cm}. On the contrary, in the case of GBFS, the dispersion increased with f_{cm}. Furthermore, no significant differences were observed in the variation of the experimental values of $f_{ct,fl}$ with f_{cm} between GPC and OC.
- The previously described standards were employed to calculate the flexural strength, $f_{ct,fl}$. The model error, expressed as the ratio of the experimental flexural strength to the calculated flexural strength, was found to be similar for GPC and OC, both in terms of the mean value μ_θ and the COV. In particular, EC2[50] and ACI318[39] gave the best results, with mean errors 0.97 and 1.03, respectively, and a percentage of points with an error of less than 20% equal to 82.8% and 77.62%,

respectively. Furthermore, it was observed that the SATS199[11] standard, although specific to GPC, led to a slightly greater error (0.83) on the safe side.

- Regarding the experimental values of the dimensionless ultimate moment μ_u, GPC showed a linear trend both for GBFS and FA data. The OC beams showed similar behavior.
- Concerning the calculation of the ultimate moment, the different models considered yield varying results. These differences can be due to the level of conservatism inherent in each model. However, when considering the same model, no significant differences were observed between GPC and OC.
- The EC2[50] and SATS199[11] models exhibited the lowest average error in the calculation of the ultimate moment, with values of 1.06 and 1.09, respectively.

A comparison of models for calculating the cracking and ultimate moments of reinforced concrete beams showed similar results for GP and Portland concretes. These conclusions were based on approximately 60 data points, and further confirmation would be useful when more data became available.

Further research is needed to expand the database and gather experimental evidence to fully understand the behavior of over-reinforced beams, where the response of the compressed concrete plays a more important role. Currently, the field is relatively under-explored, with limited specific experimental validations. In the meantime, the results obtained may be useful both for the development of new code standards specific to GPC but also for the predimensioning of structures made of these promising materials.

CONFLICT OF INTEREST STATEMENT
The authors have no conflicts of interest to declare.

DATA AVAILABILITY STATEMENT
The data that support the findings of this study are available from the corresponding author upon reasonable request.

ORCID
Erica Lenticchia https://orcid.org/0000-0002-3746-2933
Marialorenza Vescovi https://orcid.org/0009-0009-5696-315X

REFERENCES
1. Winnefeld F, Leemann A, German A, Lothenbach B. CO_2 storage in cement and concrete by mineral carbonation. Curr Opin Green Sustain Chem. 2022;38:100672. Elsevier. https://doi.org/10.1016/j.cogsc.2022.100672
2. Scrivener KL, John VM, Gartner EM, Environment U. Eco-efficient cements: potential economically viable solutions for a low-CO_2 cement-based materials industry. Cement Concrete Res. 2018;114:2–26. Elsevier. https://doi.org/10.1016/j.cemconres.2018.03.015
3. Flower DJ, Sanjayan JG. Green house gas emissions due to concrete manufacture. Int J Life Cycle Assess. 2007;12(5):282–8. Springer. 10.1065/lca2007.05.327
4. Pol Segura I, Ranjbar N, Juul Damø A, Skaarup Jensen L, Canut M, Arendt Jensen P. A review: alkali-activated cement and concrete production technologies available in the industry. Heliyon. 2023;9(5):e15718. Elsevier. https://doi.org/10.1016/j.heliyon.2023.e15718
5. Kanagaraj B, Anand N, Lukose J, Andrushia D, Lubloy E. Influence of elevated temperature exposure on the interfacial shear strength capacity of binary blended high strength self-compacting geopolymer concrete. Construction Mater. 2023;18:e01974. Elsevier. https://doi.org/10.1016/j.cscm.2023.e01974
6. Humphreys K, Mahasenan M. Toward a sustainable cement industry. Substudy 8: climate change. Switzerland: World Business Council for Sustainable Development. 2002.
7. Provis JL, van Deventer JSJ. Alkali activated materials: state-of-the-art report, RILEM TC 224-AAM. RILEM state-of-the-art reports. Netherlands: Springer. 2013 https://books.google.it/books?id=fvXHBAAAQBAJ
8. Davidovits J. Geopolymer cement a review, published in geopolymer science and technics. Vol 21. Saint-Quentin, France: Geopolymer Institute Library. 2013.
9. McLellan BC, Williams RP, Lay J, Van Riessen A, Corder GD. Costs and carbon emissions for geopolymer pastes in comparison to ordinary Portland. J Clean Prod. 2011;19(9–10):1080–1090. Elsevier. https://doi.org/10.1016/j.jclepro.2011.02.010

10. Jindal BB, Alomayri T, Hasan A, Kaze CR. Geopolymer concrete with metakaolin for sustainability: a comprehensive review on raw material's properties, synthesis, performance, and potential application. Environ Sci Pollut Res. 2023;30:25299–25324. Springer. https://doi.org/10.1007/s11356-021-17849-w
11. SA TS 199:2023. Design of geopolymer and alkali-activated binder concrete structures. Standards Australia. 2023.
12. Provis JL. RILEM TC 247-DTA round robin test: mix design and reproducibility of compressive strength of alkali-activated concretes. Mater Struct. 2019;52:1–13. Springer. doi:10.1617/s11527-019-1396-z
13. Zivica V, Palou MT, Križma M. Geopolymer cements and their properties: a review. Build Res J. 2015;61(2):85–100. De Gruyter. doi:10.2478/brj-2014-0007
14. Moon J, Bae S, Celik K, Yoon S, Kim KH, Kim KS, et al. Characterization of natural pozzolan-based geopolymeric binders. Cem Concr Compos. 2014;53:97–104. Elsevier. https://doi.org/10.1016/j.cemconcomp.2014.06.010
15. Mehta P, Monteiro PJM. Concrete: microstructure, properties, and materials. New York, NY: McGraw Hill professional. McGraw-Hill Education. 2005. https://books.google.it/books?id=Y4zlKBBW7nEC
16. Deb PS, Nath P, Sarker PK. The effects of ground granulated blast-furnace slag blending with fly ash and activator content on the workability and strength properties of geopolymer concrete cured at ambient temperature. Mater des. 2014;62:32–39. Elsevier. https://doi.org/10.1016/j.matdes.2014.05.001
17. Razak R, Abdullah M, Yahya Z, Hamid M. Durability of geopolymer lightweight concrete infilled LECA in seawater exposure. IOP conference series: materials science and engineering. Volume 267.1. Bristol: IOP Publishing. 2017;012012. https://doi.org/10.1088/1757-899X/267/1/012012
18. Pradhan P, Dwibedy S, Pradhan M, Panda S, Panigrahi SK. Durability characteristics of geopolymer concrete - Progress and perspectives. J Build Eng. 2022;59:105100. Elsevier. https://doi.org/10.1016/j.jobe.2022.105100
19. Albitar M, Ali MM, Visintin P, Drechsler M. Durability evaluation of geopolymer and conventional concretes. Construct Build Mater. 2017;136:374–85. Elsevier. https://doi.org/10.1016/j.conbuildmat.2017.01.056
20. Ansari MA, Shariq M, Mahdi F. Structural behavior of reinforced geopolymer concrete beams – a review. Mater Today Proc. 2023;1–9. Elsevier. doi:10.1016/j.matpr.2023.03.675
21. Yost JR, Radlińska A, Ernst S, Salera M, Martignetti NJ. Structural behavior of alkali activated fly ash concrete. Part 2: structural testing and experimental findings. Mater Struct. 2023;46:449–62. Elsevier. https://doi.org/10.1617/s11527-012-9985-0
22. Ambily PS, Ravisankar K, Umarani C, Dattatreya JK. Development of ultra-high-performance geopolymer concrete. Mag Concr Res. 2014;66(2):82–9. Thomas Telford Ltd. doi:10.1680/macr.13.00057
23. Devika CP, Deepthi R. Study of flexural behavior of hybrid fibre reinforced geopolymer concrete beam. Int J Sci Res(IJSR). 2015;4(7):130–5.
24. Sofi M, van Deventer JSJ, Mendis PA, Lukey GC. Engineering properties of inorganic polymer concretes (IPCs). Cement Concrete Res. 2007;37(2):251–7. Elsevier. https://doi.org/10.1016/j.cemconres.2006.10.008
25. Diaz-Loya EI, Allouche EN, Vaidya S. Mechanical properties of fly-ash-based geopolymer concrete. ACI Mater J. 2011;108(3):300–6. https://doi.org/10.14359/51682495

26. Prachasaree W, Limkatanyu S, Hawa A, Samakrattakit A. Development of equivalent stress block parameters for fly-ash-based geopolymer concrete. Arab J Sci Eng. 2014;39(12):8549–58. Springer. doi:10.1007/s13369-014-1447-2

27. Mo KH, Alengaram UJ, Jumaat MZ. Structural performance of reinforced geopolymer concrete members: a review. Construct Build Mater. 2016;120:251–64. Elsevier BV. https://doi.org/10.1016/j.conbuildmat.2016.05.088

28. Dwibedy S, Panigrahi SK. Factors affecting the structural performance of geopolymer concrete beam composites. Construct Build Mater. 2023;409:134129. Elsevier. https://doi.org/10.1016/j.conbuildmat.2023.134129

29. Lopes AV, Lopes SMR, Pinto I. Experimental study on the flexural behavior of alkali activated fly ash mortar beams. Appl Sci Switz. 2020;10(12):4379–4394. https://doi.org/10.3390/app10124379

30. Du Y, Wang J, Shi C, Hwang HJ, Li N. Flexural behavior of alkali-activated slag-based concrete beams. Eng Struct. 2021;229:111644. Elsevier BV. https://doi.org/10.1016/j.engstruct.2020.111644

31. Alex AG, Tewele TG, Kemal Z, Subramanian RB. Flexural behavior of low calcium fly ash based geopolymer reinforced concrete beam. Int J Concr Struct Mater. 2022;16(40):1–11. Springer. https://doi.org/10.1186/s40069-022-00531-x

32. Bernal SA, Mejía de Gutierrez R, Pedraza AL, Provis JL, Rodríguez ED, Delvasto S. Effect of binder content on the performance of alkali-activated slag concretes. Construct Build Mater. 2011;41(1):1–8. Elsevier. https://doi.org/10.1016/j.cemconres.2010.08.017

33. Bernal SA, Mejía de Gutierrez R, Provis JL. Engineering and durability properties of concretes based on alkali-activated granulated blast furnace slag/metakaolin blends. Construct Build Mater. 2012;33:99–108. Elsevier. https://doi.org/10.1016/j.conbuildmat.2012.01.017

34. Hardjito D, Rangan BV. Development and properties of low-calcium fly ash-based geopolymer concrete. Perth, Australia: Curtin University of Technology; 2005.

35. Sumajouw M, Rangan BV. Low-calcium fly ash-based geopolymer concrete: reinforced beams and columns. Research Report GC3. 2006;1–20. Perth, Australia: Curtin University of Technology.

36. Saranya P, Nagarajan P, Shashikala AP. Performance evaluation of geopolymer concrete beams under monotonic loading. Structure. 2019;20:560–9. Elsevier. https://doi.org/10.1016/j.istruc.2019.06.010

37. PAS 8820:2016. Construction materials. Alkali-activated cementitious material and concrete. London: Specification British Standard. 2016.

38. Kathirvel P, Kaliyaperumal SRM. Influence of recycled concrete aggregates on the flexural properties of reinforced alkali activated slag concrete. Construct Build Mater. 2016;102:51–8. Elsevier. https://doi.org/10.1016/j.conbuildmat.2015.10.148

39. ACI CODE-318-19(22). Building code requirements for struct. Concrete and commentary (reapproved 2022). Farmington Hills, Michigan: American Concrete Institute; 2019.

40. Zhang H, Wan K, Wu B, Hu Z. Flexural behavior of reinforced geopolymer concrete beams with recycled coarse aggregates. Adv Struct Eng. 2021;24(14):3281–98. SAGE Publications Inc. https://doi.org/10.1177/13694332211026224

41. AS3600. Concrete structures. Sydney: Standards Australia Limited; 2009.

42. Mehdi O, Guray A. Flexural behavior of GBFS-based geopolymer-reinforced concrete beams. Buildings. 2023;13(1):141. https://doi.org/10.3390/buildings13010141

43. EN 1992-1-1:2004. Eurocode 2: Design of concrete structures—Part 1–1: General rules and rules for buildings. CEN. 2004.

44. ACI363. State-of-the-art report on high strength concrete. Farmington Hills, MI: American Concrete Institute. 1992.

45. Ahmad SH, Shah SP. Structural properties of high strength concrete and its implications for precast prestressed concrete. PCI J. 1985;30:92–119. Precast/Prestressed Concrete Institute.

46. Swamy RN. Properties of high-strength concrete. Cem Concr Aggreg. 1986;8:33–41. CCAGDP.

47. Shehab HK, Eisa AS, Wahba AM. Mechanical properties of fly ash based geopolymer concrete with full and partial cement replacement. Construct Build Mater. 2016;126:560–5. Elsevier. https://doi.org/10.1016/j.conbuildmat.2016.09.059

48. Phoo-ngernkham T, Sata V, Hanjitsuwan S, Ridtirud C, Hatanaka S, Chindaprasirt P. Compressive strength, bending and fracture characteristics of high calcium fly ash geopolymer mortar containing portland cement cured at ambient temperature. Arab J Sci Eng. 2016;41:1263–71. Springer. https://doi.org/10.1007/s13369-015-1906-4

49. Nath P, Sarker PK. Flexural strength and elastic modulus of ambient-cured blended low-calcium fly ash geopolymer concrete. Construct Build Mater. 2017;130:22–31. Elsevier. https://doi.org/10.1016/j.conbuildmat.2016.11.034

50. EN 1992-1-1:2023. Eurocode 2: Design of concrete structures. General rules–rules for buildings, bridges and civil engineering structures. BSI. 2023.

51. Rüsch H. On the statistical quality control of concrete. Materialprüfung. 1964;6:387–94. doi:10.14359/12613

52. Torrenti JM, Frank D. On the relation between the mean compressive strength and the characteristic one. Struct Concrete. 2019;11:409–412. Wiley Online Library. doi:10.1002/suco.201900153

53. Nowak AS, Szerszen MM. Calibration of design code for buildings (ACI318): part 1-statistical models for resistance. ACI Struct. 2003;100(3):377–82. https://doi.org/10.14359/12613

54. Shibayama A, Nishiyama M. Shear strength of reinforced fly-ash-based geopolymer concrete beams with and without shear reinforcement. Structure. 2023;4(50):603–14. Elsevier. https://doi.org/10.1016/j.istruc.2023.02.060

55. Maranan GB, Manalo AC, Benmokrane B, Karunasena W, Mendis P, Nguyen TQ. Flexural behavior of geopolymer-concrete beams longitudinally reinforced with GFRP and steel hybrid reinforcements. Eng Struct. 2019;182:141–52. Elsevier. https://doi.org/10.1016/j.engstruct.2018.12.073

56. El-Sayed TA, Algash YA. Flexural behavior of ultrahigh performance geopolymer RC beams reinforced with GFRP bars. Case Stud Constr Mater. 2021;15:1–24. Elsevier. https://doi.org/10.1016/j.cscm.2021.e00604

57. George M, Benny J. Flexural behaviour of geopolymer concrete beams exposed to elevated temperatures. J Build Eng. 2018;15:311–7. Elsevier. https://doi.org/10.1016/j.jobe.2017.09.009

58. Mudimby A, Bhanuprakash D. Minimum flexural reinforcement of fly ash and GGBS based geopolymer concrete members. Mater Today Proc Elsevier. 2023;1–6. doi:10.1016/j.matpr.2023.05.031

59. Jeyasehar CA, Saravanan G, Salahuddin M, Thirugnanasambandam S. Development of fly ash based geopolymer precast concrete elements. Asian J Civ Eng (Building and Housing). 2013;14:605–15.

60. Bosco C, Caripinteri A, Debernardi PG. Minimum reinforcement in high-strength concrete. J Struct Eng. 1990;116(2):427–37. American Society of Civil Engineers. https://doi.org/10.1061/(ASCE)0733-9445(1990)116:2(427)

61. Fantilli AP, Ferretti D, Rosati G. Effect of bar diameter on the behavior of lightly reinforced concrete beams. J Mater Civ Eng. 2005;17(1):10–8. American Society of Civil Engineers. https://doi.org/10.1061/(ASCE)0899-1561(2005)17:1(10)

62. Pecce M, Fabbrocino G. Plastic rotation capacity of beams in normal and high-performance concrete. ACI Struct. 1999;96(2):290–6. American Concrete Institute. https://doi.org/10.14359/621

63. Fantilli AP, Ferretti D, Iori I, Vallini P. Flexural deformability of reinforced concrete beams: flexural cracking in RC beams. J Struct Eng. 1998;11:1041. American Society of Civil Engineers. https://doi.org/10.1061/(ASCE)0733-9445(1998)124:9(1041)

64. Fantilli AP, Ferretti D, Iori I, Vallini P. Mechanical model for failure of compressed concrete in reinforced concrete beams. J Struct Eng. 2002;128(5):637–45. American Society of Civil Engineers. https://doi.org/10.1061/(ASCE)0733-9445(2002)128:5(637)

65. Yacob NS, ElGawady MA, Sneed LH, Said A. Shear strength of fly ash-based geopolymer reinforced concrete beams. Eng Struct. 2019;196. Elsevier:109298. https://doi.org/10.1016/j.engstruct.2019.109298

66. Jang IY, Park HG, Kim SS, Kim JH, Kim YG. On the ductility of high-strength concrete beams. Int J Concr Struct Mater. 2008;2:115–22. Korea Concrete Institute. https://doi.org/10.4334/IJCSM.2008.2.2.115

67. Ferretti D. Dimensional analysis and calibration of a power model for compressive strength of solid-claybrick masonry. Eng Struct. 2020;205:110064. Elsevier. https://doi.org/10.1016/j.engstruct.2019.110064

68. Bažant ZP, Jirásek M. Creep and hygrothermal effects in concrete structures. Vol 225. Dordrecht: Springer; 2018.

69. Negahban E, Bagheri A, Sanjayan J. One-year study of restrained shrinkage and creep behaviours of geopolymer concrete. Construct Build Mater. 2023;376:131057 Elsevier. https://doi.org/10.1016/j.conbuildmat.2023.131057

70. Walraven JC, Bigaj-van Vliet A, Balazs A, Cairns J, Cervenka V, Corres H, et al. Model Code 2010-Final Draft: Volume 1. 65. (fib) International Federation for Structural Concrete. 2012.

71. ACI CODE-544 4R-11. Guide to design with fiber-reinforced concrete. Farmington Hills, Michigan: American Concrete Institute; 2018.

72. Kumar VS, Ganesan N, Indira PV. Shear strength of hybrid fibre-reinforced ternary blend geopolymer concrete beams under flexure. Materials. 2021;14(21):6634–6647. https://doi.org/10.3390/ma14216634

73. Tauqir M, Qazi UA, Khan QS, Munir MJ, Kazmi SMSK. Shear behavior of geopolymer concrete slender beams. Buildings. 2023;13(5):1191–1211. https://doi.org/10.3390/buildings13051191

74. Lin Y, Yuan Y, Wan S, Ding B, Yang C, Zong Z, et al. Flexural behaviour of reinforced onepart geopolymer concrete beams.

J Build Eng. 2024;96:110435. Elsevier. doi:10.1016/j.jobe.2024.110435

75. Bayuaji R, Darmawan MS, Wibowo B, Husin N, Subekti S. Utilization of high calcium content fly ash: flexural strength of geopolymer concrete beams in sea water environment. Open Civ Eng J. 2016;10(1):782–793. https://doi.org/10.2174/1874149501610010782

76. Cong X, Zhou W, Tan Y, Elchalakani M. Experimental investigations on the structural performance and calculation analysis of reinforced alkali-activated materials (AAMs) beams. Structure. 2022;44. Elsevier:1490–505. https://doi.org/10.1016/j.istruc.2022.08.085

77. Hammad N, ElNemr AM, Hassan HED. Flexural performance of reinforced alkali-activated concrete beams incorporating steel and structural macro synthetic polypropylene fiber. Construct Build Mater. 2022;324:126634. Elsevier. https://doi.org/10.1016/j.conbuildmat.2022.126634

78. Mansur MA, Chin MS, Wee TH. Flexural behavior of high-strength concrete beams. ACI Struct. 1997;94(6):663–674. American Concrete Institute. https://doi.org/10.14359/9726

79. Alca N, Alexander SDB, MacGregor JG. Effect of size on flexural behavior of high-strength concrete beams. ACI Struct. 1997;94(1):59–67. American Concrete Institute. https://doi.org/10.14359/461

80. Ulfkjaer JP. Experimental investigation of over-reinforced concrete beams of three different types of concrete and two different size scales. In: Mihashi H, Rokugo K, editors. Proceedings of FRAMCOS-3. Volume 3. Freiburg, Germany: AEDIFICATIO Publisher; 1998. p. 1253–60.

81. Ko MY, Kim SW, Kim JK. Experimental study on the plastic rotation capacity of reinforced high strength concrete beams. Mater Struct. 2001;34:302–11. Springer. doi:10.1007/BF02482210

82. Su J, Tan J, Li K, Fang Z. Flexural behavior of alkali-activated ultra-high-performance geopolymer concrete beams. Buildings. 2024;14(3):701. doi:10.3390/buildings14030701

83. Tran TT, Pham TM, Hao H. Experimental and analytical investigation on flexural behaviour of ambient cured geopolymer concrete beams reinforced with steel fibers. Eng Struct. 2019;200:109707 Elsevier.

84. Monfardini L, Minelli F. Experimental study on fullscale beams made by reinforced alkali activated concrete undergoing flexure. Materials. 2016;9(9):739. doi:10.3390/ma9090739

85. Monfardini L, Facconi L, Minelli F. Experimental tests on fiber-reinforced alkali-activated concrete beams under flexure: some considerations on the behavior at ultimate and serviceability conditions. Materials. 2019;12(20):3356. https://doi.org/10.3390/ma12203356

AUTHOR BIOGRAPHIES

Erica Lenticchia, Department of Structural, Geotechnical and Building Engineering, Politecnico di Torino, C.so Duca degli Abruzzi 24, 10129, Torino, Italy. erica.lenticchia@polito.it

Marialorenza Vescovi, Department of Engineering and Architecture, University of Parma, Parma, Italy. marialorenza.vescovi@unipr.it